Hindawi
Journal of Control Science and Engineering
Volume 2023, Article ID 3373863, 11 pages
https://doi.org/10.1155/2023/3373863

Research Article

Modified Passivity-Based Control for LCL-Filtered Grid-Tied Inverter with Output Admittance Reshaping

Han Wang, Gang Shi, Jianwen Zhang, Miao Zhu, and Xu Cai

The Key Laboratory of Control of Power Transmission and Conversion of Ministry of Education, Shanghai Jiao Tong University, Shanghai 200240, China

Correspondence should be addressed to Jianwen Zhang; icebergzjw@sjtu.edu.cn

Received 12 July 2022; Revised 19 October 2022; Accepted 29 October 2022; Published 6 January 2023

Academic Editor: Carlos-Andrés García

As a nonlinear control method, the Euler–Lagrange- (EL-) based passivity-based control (PBC) has been studied for grid-tied converters based on energy function to achieve better performance. However, the EL-based PBC method is dependent on an accurate mathematical model. In the traditional EL-based PBC research for LCL-filtered grid-tied inverter, the effect of the digital control delay is rarely considered and the stability under the grid impedance uncertainties is not discussed, especially in the capacitive grid or complex weak grid. To address these concerns, this study proposes a modified EL-based PBC method based on the output admittance reshaping for LCL-filtered grid-tied inverters. The system' passive region is expanded by adding capacitor current feedback loop up to the Nyquist frequency. The potential resonance is thus eliminated irrespective of the grid impedance. Additionally, the stable region and control parameters design methods of the modified EL-based PBC method with inverter-side control are also carried out. To verify the correctness of the theoretical analysis, both simulation and experimental results are investigated from a 3 kW grid-tied inverter prototype.

1. Introduction

Under the influence of energy shortage and global warming, the distributed renewable energy generation system has become more and more important. Generally, renewable energy resources are interfaced to the power grid by grid converters [1, 2]. To get a better dynamic performance and attenuate the injected current harmonics effectively, the LCL filter is frequently selected to filter out switching harmonics caused by pulse width modulation (PWM) [3]. Even though the LCL filter can save total inductance compared to the L filter, the inherent resonance problems caused by the high-order filter may destabilize the entire system and pose challenges to the design of the controller, especially when the variations of grid impedance are considered.

Proportional-integral (PI) and proportional-resonant (PR), as conventional linear control methods, are usually implemented with passive damping [4–6] or active damping [7–12] techniques to eliminate the possible resonance problems. The passive damping method involves directly adding physical resistors in the filter circuit, which will certainly lead to extra losses and complexity to the resistor design. The active damping method is usually achieved by using state feedback variables to construct a virtual resistor, but additional sensors or complex algorithms will be necessary in the realization. What is more is that filter-based damping and inherent damping methods are also proposed with the digital implementation [13, 14]. Given the time delay of $1.5T$, where T is the sampling period, it was found that if the LCL resonance frequencies are placed below one-sixth of the sampling frequency, the extra damping is not required for inverter-side current control. Instead, for the grid-side current control, the LCL resonance frequencies should be placed above one-sixth of the sampling frequency. But control effects of these damping methods are strongly dependent on grid impedance, LCL filter parameters, and sampling frequency [15].

Apart from the linear control methods, some nonlinear control methods have been increasingly studied for DC-DC converters and DC-AC converters considering the nonlinear

characteristics of converters, [16] including passivity-based control (PBC), [17–20] predictive control (PC), [21, 22] sliding mode control (SMC), and so on [23, 24]. Among these nonlinear control strategies, the passivity-based control (PBC) approach has attached wide attention owing to its capability to realize better performances and strong robustness based on the energy dissipation and modification methods. The PBC method was first proposed in the electrical system by Ortega et al. [25] which described the physical system by the Euler–Lagrange (EL) model or port-controlled Hamiltonian systems with dissipation (PCHD) equation. The error energy function based on Lyapunov's theory is normally constructed and the controller is designed with damping injection. The authors in [26] adopted the PBC-based EL model to suppress the low-frequency oscillations with L filter in the railway power system. The authors in [17] implemented the passivity-based decoupling control for the neutral point clamped photovoltaic inverter to gain parameters perturbations, but the grid impedance is not considered. In order to decrease the steady-state error and improve the robustness of the system, a design procedure of the damping gains for the LCL-filtered grid-tied inverter based on PBC is proposed in reference [18], but the delay is approximated. In some cases, grid-tied inverters are normally interfaced together to the grid at the point-of-common-coupling (PCC) in the distributed generation system, and the equivalent grid impedance could be capacitive in long cable or more complex grid [27]. The conventional EL-based PBC methods of the LCL-type filter-based grid-tied voltage source inverter (VSI) system rarely take the capacitive grid condition and digital delay into consideration [28, 29]. The probably varying resonance frequencies of the system will easily lead to interactive resonances in the digital implementation. Therefore, the controller design of PBC becomes very important facing the complex grid impedance.

Although EL-based PBC is defined as the nonlinear control based on energy dissipation, the control law can be implemented with linear control block, which combine feedforward control, negative feedback control, and decoupling control. To oppose grid impedance uncertainties, the impedance-based method has been applied to assess stability and dynamic interactions of paralleled VSIs systems with linear control methods [21, 30–33]. The authors in [33] analyzed passive characteristics of the single-loop grid-side current control and converter-side current control with traditional PI or PR, but it is hard to ensure all regions passively. Inspired by the previous work, the modified EL-based PBC strategy has the following contributions:

(i) For conventional EL-based PBC, the passivity is only ensured for inverter itself when designing the control law. Nonpassive regions caused by the control delay of the system and grid impedance are not considered. In this study, the impedance model of EL-based PBC-based LCL-filtered VSI with control delay is derived and it reveals that the inverter output admittance is not passive with the EL-based PBC method.

(ii) It still has lack of the specific design method for the parameters of EL-based PBC. In this study, a frequency-domain design method is implemented to ensure the stability of the inverter under the complex grid impedance.

(iii) As compared to conventional linear PI control, this study proposed a simple admittance reshaping strategy for LCL-filtered VSI with EL-based PBC, which easily ensure the passivity of the inverter output admittance up to the Nyquist frequency.

This study is organized as follows: First, the Euler–Lagrange model is built for LCL-filtered three-phase VSI, and EL-based PBC control law is deduced with inverter-side current control. Then, the impedance of LCL-filtered three-phase grid-tied VSI with EL-based PBC is analyzed and control output admittance is deduced. Based on the frequency-domain passivity theory, the influence of time delay and the nonpassive regions of the inverter output admittance are identified. Then, the phase reshaping is applied to expand the passive region with the capacitor current feedback method. The proposed strategy can achieve passive output admittance up to the Nyquist frequency with inverter-side current control. Finally, simulated and experimental results are presented to confirm the performance and correctness of the proposed control method.

2. EL-Based PBC Control for LCL-Filtered Three-Phase Grid-Tied Inverter

2.1. System Modelling. The structure of the three-phase LCL-filtered VSI system with the PBC controller is illustrated in Figure 1. The LCL filter is expressed by L_1, C, and L_2, where R_1 and R_2 denote the equivalent parasitic resistances of L_1 and L_2, respectively. The output current and voltage of inverter created by PWM are notated as i_1 and u_i. u_C and i_c represent the voltage and current of capacitor, respectively. In this study, the inverter-side current is regulated and synchronized with capacitor voltage. U_{dc} is noted as the DC link voltage and i_2 is the injected grid current. v_{pcc} is the PCC joint voltage. Z_g is the impedance of the grid, which is composed of inductor L_g and capacitor C_g. The mathematical model of the LCL-filtered three-phase VSI can be described by applying Kirchhoff voltage law (KVL). The three-phase variables are usually formulated in the synchronously rotating dq-coordinate frame, and then, the system voltage equations are expressed in function (1), where ω represents the grid angular frequency. The three-order LCL system can be decomposed into three subsystems to decouple the cascaded three-order LCL system in d-channel and q-channel, respectively.

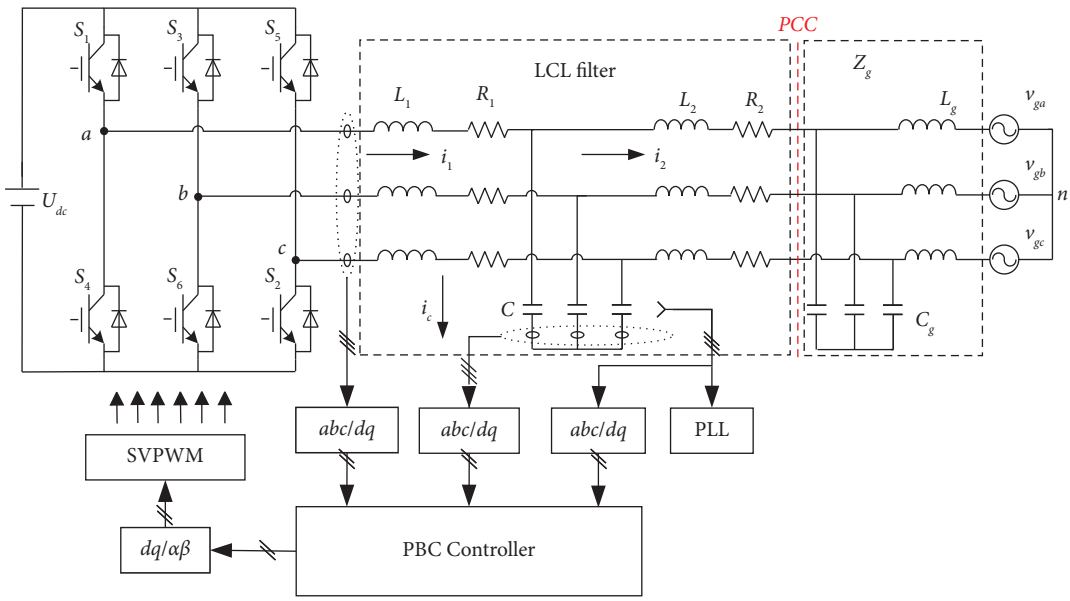

Figure 1: Configuration of LCL-filtered three-phase grid-tied VSI based on PBC with inverter-side current control.

$$\begin{cases} L_1\dfrac{\mathrm{d}i_{1d}}{\mathrm{d}t} + R_1 i_{1d} = u_{id} + \omega L_1 i_{1q} - u_{Cd} \\ L_1\dfrac{\mathrm{d}i_{1q}}{\mathrm{d}t} + R_1 i_{1q} = u_{iq} - \omega L_1 i_{1d} - u_{Cq} \end{cases},$$

$$\begin{cases} L_2\dfrac{\mathrm{d}i_{2d}}{\mathrm{d}t} + R_2 i_{2d} = u_{Cd} + \omega L_2 i_{2q} - v_{\mathrm{pccd}} \\ L_2\dfrac{\mathrm{d}i_{2q}}{\mathrm{d}t} + R_2 i_{2q} = u_{Cq} - \omega L_2 i_{2d} - v_{\mathrm{pccq}} \end{cases},$$

$$\begin{cases} C\dfrac{\mathrm{d}u_{Cd}}{\mathrm{d}t} + i_{2d} = i_{1d} + \omega C u_{Cq} \\ C\dfrac{\mathrm{d}u_{Cq}}{\mathrm{d}t} + i_{2q} = i_{1q} - \omega C u_{Cd}. \end{cases} \quad (1)$$

As an important part of the nonlinear PBC theory, the EL method is used to describe the system model. Since inverter-side current is controlled, the filter capacitor and filter inductor can be seen as together with the grid impedance. So, only the model of the inverter-side current variables should be designed for the simplification. The first two equations of function (1) can be written in the form with the EL model as follows:

$$M\dot{x} + Jx + Rx = u, \quad (2)$$

where

$$M = \begin{bmatrix} L_1 & 0 \\ 0 & L_1 \end{bmatrix},$$
$$J = \begin{bmatrix} 0 & -\omega L_1 \\ \omega L_1 & 0 \end{bmatrix},$$
$$R = \begin{bmatrix} R_1 & 0 \\ 0 & R_1 \end{bmatrix}, \quad (3)$$
$$x = \begin{bmatrix} i_{1d} & i_{1q} \end{bmatrix}^T,$$
$$u = \begin{bmatrix} u_{id} - u_{Cd} \\ u_{iq} - u_{Cq} \end{bmatrix}.$$

Equation (2) is seen as the state equation, in which i_{1d} and i_{1q} represent the corresponding d-component and q-component of state variable i_1, respectively. M and R are the positive definite diagonal matrices, where R represents the internal energy dissipation characteristics of the system; J is the skew-symmetric matrix which describes the internal coupled structure between d-axis and q-axis current component, and $J = -J^T$; u is the control input matrix, which represents the system and external energy input.

2.2. Traditional EL-Based PBC Control Law and Damping Injection. The system is considered strictly passive if there exists a positive definite function $Q(x)$, and a nonnegative storage function $V(x)$ can satisfythe equation [17].

$$V[x(t)] - V[x(0)] \le \int_0^t u^T y d\tau - \int_0^t Q(x) d\tau, \quad t > 0, \tag{4}$$

or

$$\dot{V}[x] \le u^T y - Q(x), \tag{5}$$

where u and y are noted as system input and output variables, respectively. $u^T y$ is the injected rate of external energy. Function (4) indicates that the sum of the increased energy of the system is always less than the sum of the external injected energy. For the LCL-filtered grid-tied inverter, the system energy storage function is defined as follows:

$$V(x) = \frac{1}{2} x^T M x, \tag{6}$$

where positive definite function $V(x)$ represents the energy storage of the internal system. Combining with (2), the time derivative of system energy function (6) is taken. Then, it deduces the following:

$$\dot{V}(x) = x^T M \dot{x} = x^T (u - Jx - Rx) = x^T u - x^T R x. \tag{7}$$

Letting $y = x$, $Q(x) = x^T R x$, and combining with function (5), it can be seen that the system is passive. The integration term $\int_0^t x^T u dt$ is the external supply energy of the system. $\int_0^t x^T R x dt$ is the dissipative term caused by the parasitic resistance of the system.

According to the passivity situation, the object described in (2) is strictly passive where the EL-based PBC can be adopted to design the controller. For inverter-side current control, the current reference variables can be defined as follows:

$$x^* = \left[i_{1d}^*, i_{1q}^* \right]^T. \tag{8}$$

The error vector of the current is denoted as $x_e = x^* - x$; then, an error EL equation is obtained by (2) as

$$M(\dot{x}^* - \dot{x}_e) + J(x^* - x_e) + R(x^* - x_e) = u. \tag{9}$$

$$M\dot{x}^* + Jx^* + Rx^* - u = M\dot{x}_e + Jx_e + Rx_e. \tag{10}$$

If the error x_e is equal to zero, the desired control objective and stable equilibrium point will happen. A positive damping matrix R_d can be added to the error EL model (10) to accelerate the error to reach zero. The injected damping and new dissipation term are described as

$$\begin{aligned} R_d &= diag[\, r_1 \;\; r_1 \,], \\ R_{new} &= R + R_d, \end{aligned} \tag{11}$$

where $r_1 > 0$. Taking function (11) into the error equation, the new error equation with injected damping is rewritten as

$$M\dot{x}_e + Jx_e + R_{new} x_e = M\dot{x}^* + J\dot{x}^* + Rx^* + R_d x_e - u = \zeta. \tag{12}$$

In this study, ζ is set as Jx_e to eliminate the coupling terms of system [26]. Thus, the control law from (12) is derived as follows:

$$\begin{cases} u_d = L_1 \dfrac{di_{1d}^*}{dt} - \omega L_1 i_{1q} + R_1 i_{1d}^* + r_1 (i_{1d}^* - i_{1d}) + u_{Cd}, \\ u_q = L_1 \dfrac{di_{1q}^*}{dt} + \omega L_1 i_{1d} + R_1 i_{1q}^* + r_1 (i_{1q}^* - i_{1q}) + u_{Cq}. \end{cases} \tag{13}$$

According to the analysis mentioned before, the controller diagram in Laplace domain of the grid-tied VSI with the EL-based PBC method is depicted in Figure 2, where L_1 and R_1 present the actual values of the LCL filter physical model, and L_{1e} and R_{1e} present the designed LCL filter parameters in the controller. In the implementation, r_1 can be substituted by PI controller to reduce the steady-state error. $e^{-1.5Ts}$ indicates the computational and modulation delays, and T is the sampling period [9]. Since the delays are not considered in the design of the conventional EL-based PBC controller, dissipative properties of its output admittance should be investigated in the following discussion.

3. Impedance Model and Stability Analysis of LCL-Filtered Grid-Tied VSI with EL-Based PBC

3.1. Impedance Model of LCL-Filtered Grid-Tied VSI with EL-Based PBC. The common Norton equivalent model of the LCL-filtered grid-tied inverter is shown in Figure 3. $Y_o(s)$ is the control output admittance for the inverter-side current control and Z_g is the grid impedance mentioned in Figure 1.

The voltage across the filter capacitor can be regarded as the disturbance input. Then, overall closed-loop response of the inverter current loop can be described with two parts as follows:

$$i_1 = G(s) i_1^* - Y_o(s) u_C, \tag{14}$$

where $G(s)$ is the closed-loop transfer function from output current to reference current, which determines the dynamic response and steady-state error of LCL-filtered grid-tied VSI with inverter-side current control. Filter capacitor and filter inductor are regarded as external grid impedance, together with grid admittance Z_g. Y_{gt} is the total external grid admittance, as shown in the following function.

$$Y_{gt}(s) = \frac{s^2 L_g C_g + 1}{s^3 C_g L_g L_2 + s(L_2 + L_g)} + sC. \tag{15}$$

Based on the closed-loop response of the inverter current in (14), the closed-loop inverter current response seen from the grid voltage can be deduced in the following equation.

$$i_1 = \frac{G(s)}{1 + Y_o / Y_{gt}} i_i^* - \frac{Y_o(s)}{1 + Y_o / Y_{gt}} v_g. \tag{16}$$

Function (16) can also be divided in two parts. The dynamic response and external disturbance stability of the whole system are also related to the transfer function $Y_o(s)/Y_{gt}(s)$. $Y_o(s)$ and $Y_{gt}(s)$ should be both passive to guarantee the stability of the interconnected inverters and the grid system. Since $Y_{gt}(s)$ is composed of resistor, inductor, and capacitor, it is obviously a passive network. Thus, the

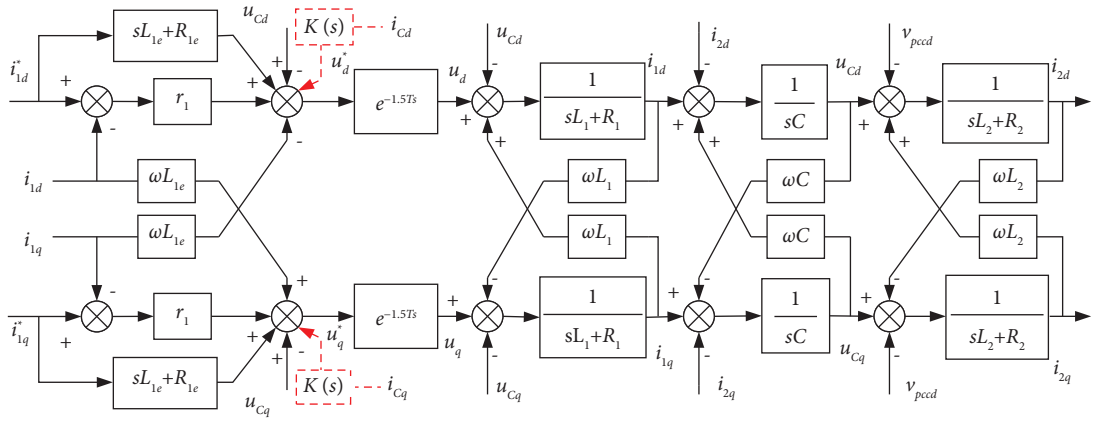

Figure 2: Control structure for LCL-filtered three-phase grid-tied VSI with EL-based PBC with inverter-side current control.

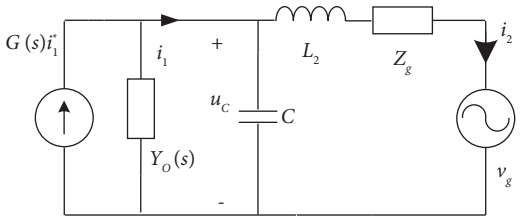

Figure 3: Norton equivalent model.

Table 1: System parameters.

Symbols	Components	Value
U_{dc}	DC link voltage	350 V
L_1	Inverter-side inductor	1.2 mH
L_2	Grid-side inductor	1.2 mH
C	Capacitor of LCL filter	6 μF
f_s	Sampling frequency	10 kHz
f_{sw}	Switching frequency	10 kHz
R_1, R_2	Equivalent resistance of filter inductor L_1, L_2	0.1 Ω, 0.1 Ω
V_g	Grid voltage	110 V (RMS)
f_o	Grid frequency	50 Hz
C_g	Grid capacitor	3 μF
L_g	Grid inductor	3.6 mH

impedance model of inverter-side control with EL-based PBC should be derived to make sure that $Y_o(s)$ is passive.

The current and voltage equations of the LCL filter can be obtained from Kirchhoff law, which are given by following matrices:

$$\begin{bmatrix} i_{1d} \\ i_{1q} \end{bmatrix} = \begin{bmatrix} 0 & \omega L_1 \\ -\omega L_1 & 0 \end{bmatrix} \begin{bmatrix} D & 0 \\ 0 & D \end{bmatrix} \begin{bmatrix} i_{1d} \\ i_{1q} \end{bmatrix} + \begin{bmatrix} D & 0 \\ 0 & D \end{bmatrix} \begin{bmatrix} u_d \\ u_q \end{bmatrix}, \tag{17}$$

where $\omega = 2\pi f$, $D = 1/(sL_1 + R_1)$. Based on Figure 2, the inverter side current control law u^* based on EL-based PBC in d-q axis is written as follows:

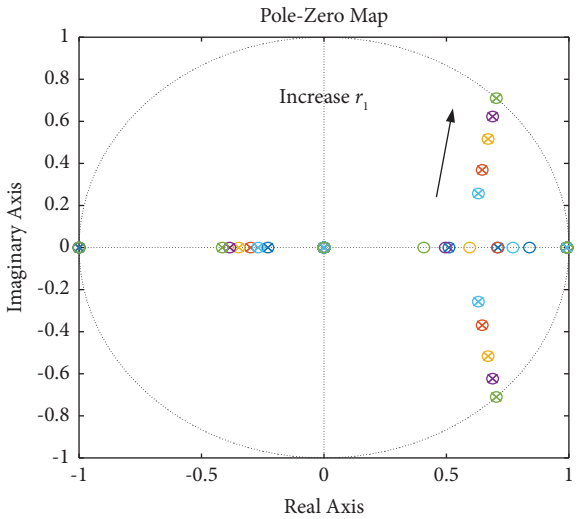

Figure 4: Closed-loop poles, when r_1 is increased from 0 to 12.

$$\begin{bmatrix} u_d^* \\ u_q^* \end{bmatrix} = \begin{bmatrix} E & 0 \\ 0 & E \end{bmatrix} \begin{bmatrix} i_{1d}^* \\ i_{1q}^* \end{bmatrix} - \begin{bmatrix} r_1 & \omega L_{1e} \\ -\omega L_{1e} & r_1 \end{bmatrix} \begin{bmatrix} i_{1d} \\ i_{1q} \end{bmatrix} + \begin{bmatrix} u_{Cd} \\ u_{Cq} \end{bmatrix}, \tag{18}$$

where $E = sL_{1e} + R_{1e} + r_1$. Considering the computing delay and sampling delay, the control law u after delay is written in function (19) and $T = 1/f_s$.

$$\begin{bmatrix} u_d \\ u_q \end{bmatrix} = e^{-1.5Ts} \begin{bmatrix} u_d^* \\ u_q^* \end{bmatrix}. \tag{19}$$

Combined with functions (17)–(19), the closed-loop transfer function matrix of the system is deduced in (20). Then, the performance of the LCL-filtered three-phase grid-tied inverter with EL-based PBC with inverter-side current control can be evaluated.

$$\begin{bmatrix} i_{1d} \\ i_{1q} \end{bmatrix} = \frac{DEe^{-1.5Ts}}{\left(1 + r_1 De^{-1.5Ts}\right)^2 + \left(\omega L_1 D - \omega L_{1e} De^{-1.5Ts}\right)^2} \begin{bmatrix} 1 + r_1 De^{-1.5Ts} & \omega L_1 D - \omega L_{1e} De^{-1.5Ts} \\ -\omega L_1 D + \omega L_{1e} De^{-1.5Ts} & 1 + r_1 De^{-1.5Ts} \end{bmatrix} \begin{bmatrix} i_{1d}^* \\ i_{1q}^* \end{bmatrix} + \frac{D\left(e^{-1.5Ts} - 1\right)}{\left(1 + r_1 De^{-1.5Ts}\right)^2 + \left(\omega L_1 D - \omega L_{1e} De^{-1.5Ts}\right)^2} \begin{bmatrix} 1 + r_1 De^{-1.5Ts} & \omega L_1 D - \omega L_{1e} De^{-1.5Ts} \\ -\omega L_1 D + \omega L_{1e} De^{-1.5Ts} & 1 + r_1 De^{-1.5Ts} \end{bmatrix} \begin{bmatrix} u_{Cd} \\ u_{Cq} \end{bmatrix}. \tag{20}$$

Due to the steady-state $i_{1d}/i_{1d}^* = 1$, d-q axis coupling terms are neglected. Then, $G(s)$ and $Y_o(s)$ of the proposed method can be expressed in the following equations.

$$G(s) = \frac{DEe^{-1.5ts}\left(1 + r_1 De^{-1.5Ts}\right)}{\left(1 + r_1 De^{-1.5Ts}\right)^2 + \left(\omega L_1 D - \omega L_{1e} De^{-1.5Ts}\right)}, \tag{21}$$

$$Y_o(s) = \frac{-D\left(e^{-1.5ts} - 1\right)\left(1 + r_1 De^{-1.5Ts}\right)}{\left(1 + r_1 De^{-1.5Ts}\right)^2 + \left(\omega L_1 D - \omega L_{1e} De^{-1.5Ts}\right)}. \tag{22}$$

3.2. Passivity-Based Stability Analysis. Passivity theory can also be described in frequency domain based on the impedance model, which provided a sufficient but not necessary condition. To define a passive system, the closed-loop transfer function $G(s)$ should have no RHP poles, and it is internally stable. Then, the output admittance of the control loop, $Y(j\omega)$, should have a nonnegative real part or the phase of $Y(j\omega)$ within $[-90, 90]$, i.e., Re $\{Y(j\omega)\} \geq 0 \Leftrightarrow \arg\{Y(j\omega)\} \in [-90^\circ, 90^\circ]$, $\forall \omega > 0$.

Hence, to make the LCL-filtered three-phase grid-tied VSI to be passive considering the control delay, the internal stability of the system should be analyzed. The system parameters used for analysis are described in Table 1.

Figure 4 indicates the z-domain zeros-poles based on the damped close-loop plant to illustrate the boundary for internal stability. As long as the gain r_1 is less than 12, all the poles are placed inside the stable circle. It can be noticed that the poles move inside and a better internal stability can be obtained with less damping coefficient r_1. But the dynamic response and the bandwidth will be better with larger r_1. Figure 5 shows the step responses of $G(s)$ with different r_1 to help with the selecting of r_1. The suitable range of r_1 can be selected between 3 and 6 based on the performance of overshoot and setting time.

The passive characteristic of the system has been analyzed when applying the EL-based PBC in Section 2. However, the delay and control will bring the nonpassive region in the digital realization. It is worth noting that the grid impedance values can change in a wide range depending on the situation. Thus, the external interaction stability with grid impedance should be evaluated. Based on the frequency-domain passivity theory, the EL-based PBC output admittance can be deduced to analyze the passivity of the overall system. The influences of coefficient r_1 on the output admittance passivity region of the EL-based PBC method and system stability are shown in Figure 6, and $Y_{gt}(s)$ is the equivalent network admittance.

The magnitude of $Y_o(s)$ is sufficiently small in low frequency range, which means the inverter rejection capability for grid voltage harmonics is sufficient with the adoption of the EL-based PBC method. It can be seen that the equivalent negative resistor also exists which makes the system unstable with the traditional EL-based PBC control. Compared to traditional PI control, the $1/6f_s$ is no longer the critical frequency for the *LCL*-filtered grid-tied VSI with the EL-based PBC method. When r_1 is greater than 14, the phase curve of Y_o crosses 90 degree no matter what the Y_{gt} value is. Thus, r_1 should be chosen between the region 4 and 9 to achieve a better stability margin, also considering internal stability and system dynamic response. Here, r_1 is selected as 6.

4. Passivity-Based Damping Enhancement Method

To narrow the nonpassive region, the damping enhancement method should be investigated. To reshape the control output admittance, the capacitor current feedback is adopted for EL-based PBC in this study, as shown in Figure 2 with dotted box, and is given as follows:

$$I_c = sCu_C. \tag{23}$$

After adding capacitor current feedback, the function (18) is replaced by the following function.

$$\begin{bmatrix} u_d \\ u_q \end{bmatrix} = \begin{bmatrix} E & 0 \\ 0 & E \end{bmatrix} \begin{bmatrix} i_{1d}^* \\ i_{1q}^* \end{bmatrix} - \begin{bmatrix} r_1 & \omega L_{1e} \\ -\omega L_{1e} & r_1 \end{bmatrix} \begin{bmatrix} i_{1d} \\ i_{1q} \end{bmatrix} + \begin{bmatrix} u_{Cd} \\ u_{Cq} \end{bmatrix} - KsC \begin{bmatrix} u_{Cd} \\ u_{Cq} \end{bmatrix}. \tag{24}$$

Thus, system admittance equation is replaced by function (25), where K is the feedback coefficient.

$$Y_o(s) = \frac{-D\left((1 - KsC)e^{-1.5Ts} - 1\right)\left(1 + r_1 De^{-1.5Ts}\right)}{\left(1 + r_1 De^{-1.5Ts}\right)^2 + \left(\omega L_1 D - \omega L_{1e} De^{-1.5Ts}\right)^2}. \tag{25}$$

The Bode plot of the control output admittance with capacitor current proportional feedback is shown in Figure 7. The proportional coefficient k should be negative to ensure the stability of the system. It can be seen that the nonpassive regions of high frequency are narrowed after adding proportional feedback, and a better mitigation effect is achieved with higher feedback coefficient, but the nonpassive region cannot be totally removed. Even worse, it will cause another nonpassive in the low and middle frequencies if the feedback value is high.

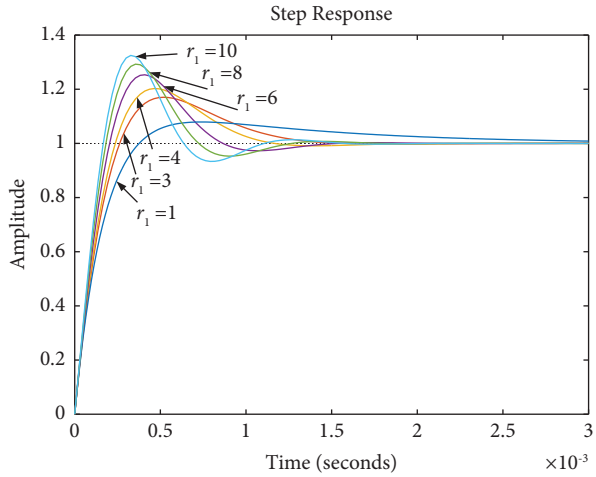

Figure 5: Step responses of closed-loop $G(s)$ when $r_1 = 1, 3, 4, 6, 8, 10$.

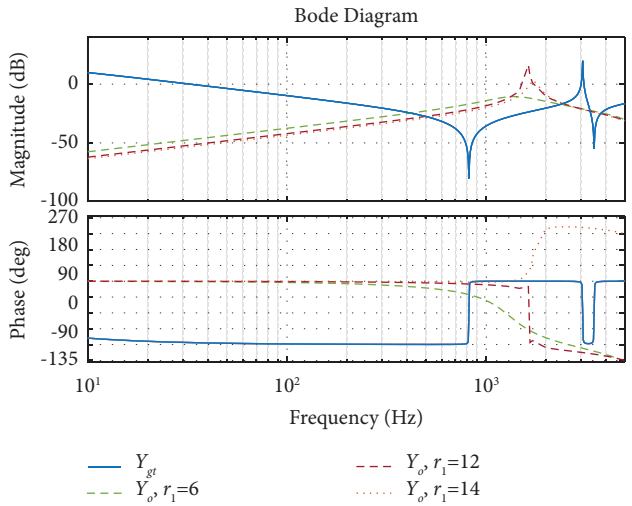

Figure 6: The output admittance $Y_o(s)$ with different r_1 and the equivalent network admittance $Y_{gt}(s)$.

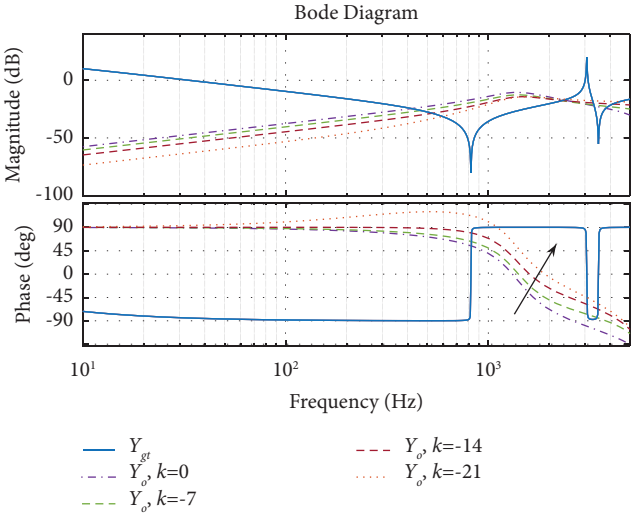

Figure 7: The output admittance $Y_o(s)$ with different proportional feedback coefficients and the equivalent network admittance $Y_{gt}(s)$.

In order to compensate the negative effect of delays on the system phase in the high frequency, there are many filter-based methods, such as the lead-lag compensator, high pass filter (HPF), and the infinite impulse response (IIR) filter with the phase lead characteristics [34]. But it is hard to achieve all passive within the Nyquist frequency for the traditional PI controlled grid-connected inverter [9].

Here, to extend the passivity range of the output phase, a simple high pass filter is added to the capacitor current feedback loop based on EL-based PBC. The $K(s)$ is expressed as follows:

$$K(s) = \frac{ks}{(s+a)}. \tag{26}$$

The Bode plots in Figure 8 show that the high pass has a negligible effect at low frequency, but it can compensate the nonpassive region near to the Nyquist frequency or even higher. The corner frequency a is selected as 10000 to reach the compensation effect. The coefficient k cannot be too high or too small, and it is selected as −7 to keep the consistency with the proportional feedback method. Here, $L_g = 3.6$ mH, $C_g = 2\,\mu$F, and the potential unstable point is around 3000–4000 Hz. If the L_g or C_g varies, the interaction points could move forward or backward. Within Nyquist frequency, the modified EL-based PBC control can ensure the robustness of the LCL-filtered grid-tied inverter in the weak grid.

5. Simulations and Experimental Studies

5.1. Simulation Results. The overall control structure is depicted in Figure 2. Based on the theoretical analysis mentioned above, a three-phase LCL-filtered grid-tied inverter system with EL-based PBC is simulated to verify the effectiveness of the proposed control method using Matlab/Simulink platform. The detailed parameters of the system and controller are shown in Tables 1 and 2, respectively.

Figure 9 depicts the simulated grid currents of the LCL-filtered three-phase grid-tied inverter system with EL-based PBC control when different feedback strategies of capacitor current are enabled in the strong grid. At the beginning, the system is stable with proposed HPF feedback and the system is stable when k feedback is enabled at 0.12 s. However, the grid currents start to oscillate when damping controllers are deactivated at 0.16 s. Figure 10 illustrates Bode plot of the control output admittance $Y_o(s)$ and the equivalent network admittance $Y_{gt}(s)$ without capacitor current feedback when $L_g = 0$ and $C_g = 0$.

It can be seen that there is one interaction point of $Y_o(s)$, and $Y_{gt}(s)$ falls into the nonpassive region, where the phase of $Y(j\omega)$ is out of the region [−90, 90]. Hence, three-phase LCL-filtered grid-tied VSI with EL-based PBC could be unstable due to the influence of the delay and the damping enhancement method should be performed.

Figure 11 shows the simulated grid currents of the LCL-filtered three-phase grid-tied inverter system with different capacitor current feedback methods when $L_g = 3.6$ mH and $C_g = 0$. The system keeps stable with two

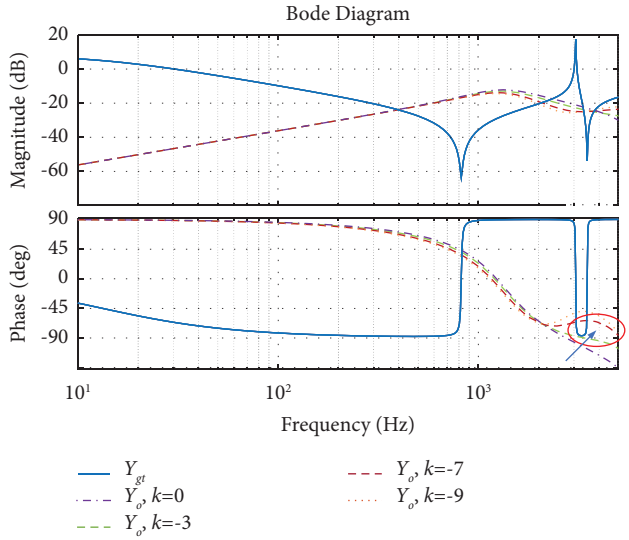

Figure 8: The output admittance $Y_o(s)$ with different HPF feedback coefficients and the equivalent network admittance $Y_{gt}(s)$.

Table 2: Controller parameters.

Symbols	Components	Value
k	Gain of capacitor current feedback	−7
r_1	Damping gain	6

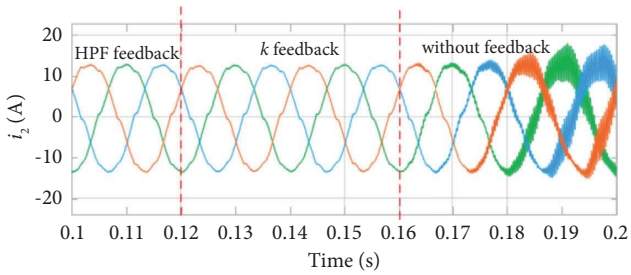

Figure 9: Simulated grid currents with different capacitor current feedback methods when $L_g = 0$ and $C_g = 0$.

different capacitor current feedback methods in the inductive grid impedance.

The simulated grid currents of the three-phase LCL-filtered grid-tied inverter system with different capacitor current feedback methods are shown in Figure 12, when $L_g = 3.6$ mH and $C_g = 2\,\mu$F. As mentioned before, as shown in Figure 7, the system nonpassive region can be narrowed with higher k, but cannot be fully compensated before Nyquist frequency with k feedback. Here, the k is selected as −7, where the smaller C_g would bring higher interaction resonance frequency and easier stimulate oscillations. In Figure 12, the system is unstable in capacitive grid with $L_g = 3.6$ mH and $C_g = 2\,\mu$F and then turns to stability at the time instant of 0.12 s with the proposed HPF feedback.

5.2. Experimental Results. Apart from the simulated results, the experimental results are also investigated on a 3 kW

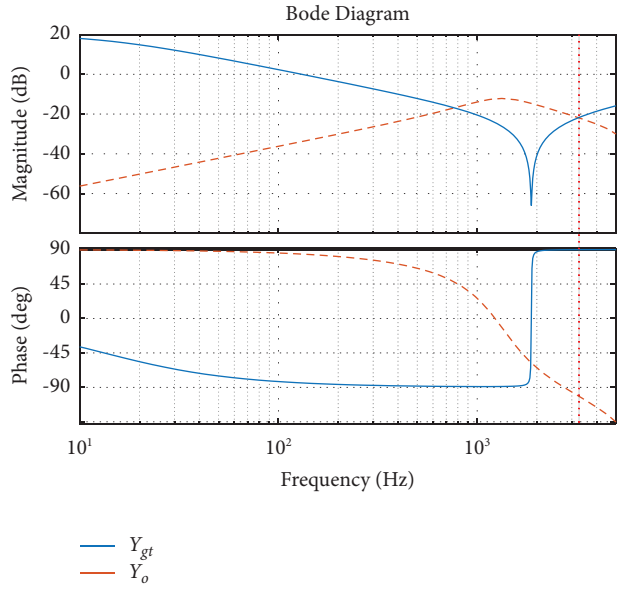

Figure 10: The output admittance $Y_o(s)$ without feedback and the equivalent network admittance $Y_{gt}(s)$ when $L_g = 0$ and $C_g = 0$.

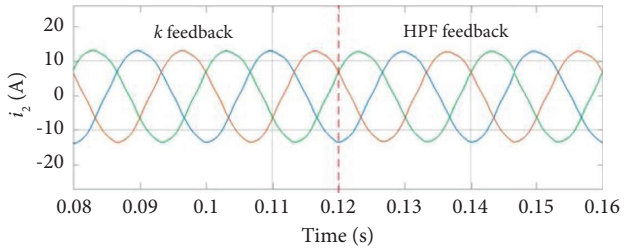

Figure 11: Simulated grid currents of the three-phase LCL-filtered grid-tied inverter system with different capacitor current feedback methods when $L_g = 3.6$ mH and $C_g = 0$.

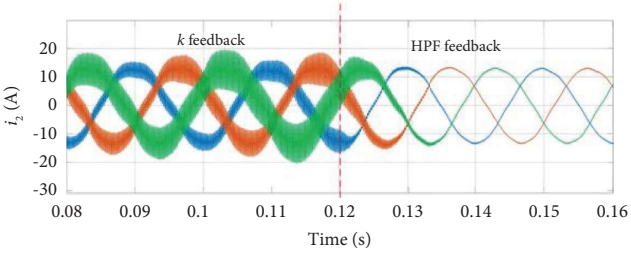

Figure 12: Simulated grid currents with different capacitor current feedback methods when $L_g = 3.6$ mH and $C_g = 2\,\mu$F.

three-phase LCL-filtered grid-tied inverter system to validate the performance of the proposed control method. The hardware prototype is with Danfoss FC302 inverter, as shown in Figure 13. The proposed control scheme and sampling data are implemented in a dSPACE DS1202 controller. The DC voltage is supplied with a Chroma 62150H-600S, and the power grid is generated by a Chroma 61830 three-phase grid simulator.

System parameters adopted in the experiments are same as the simulations, as shown in Table 1. HPF feedback

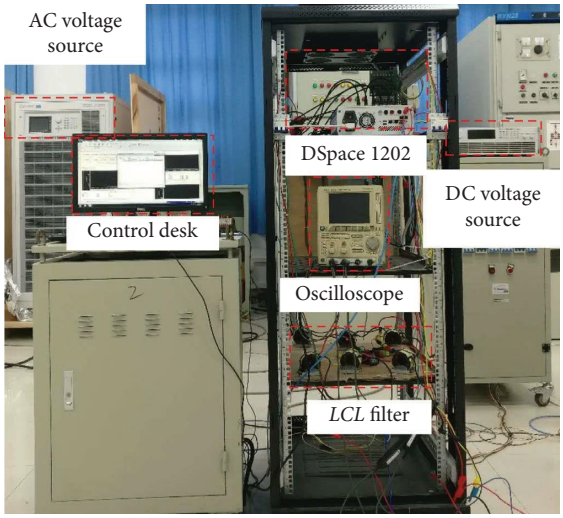

Figure 13: Experimental system prototype.

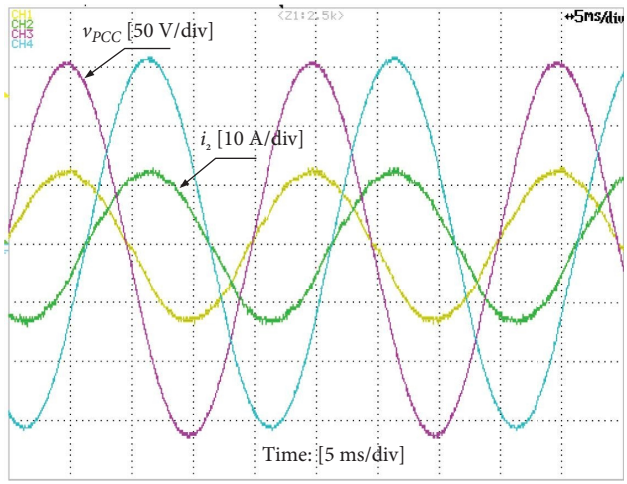

Figure 14: Experimental waveforms with proposed control when $L_g = 3.6$ mH and $C_g = 2\,\mu$F.

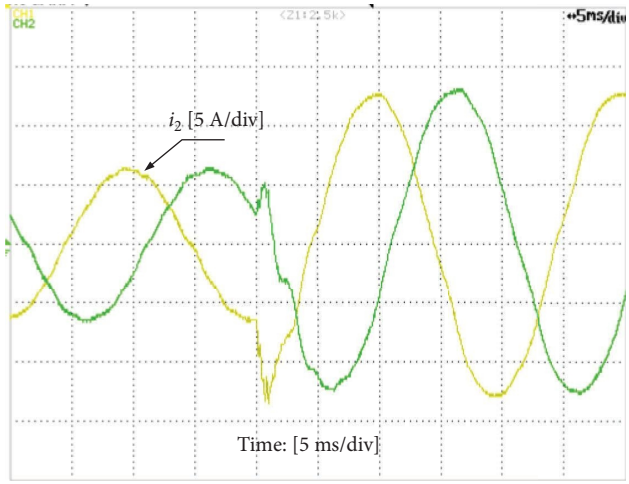

Figure 15: Measured waveforms of grid currents with reference step when $L_g = 3.6$ mH and $C_g = 2\,\mu$F.

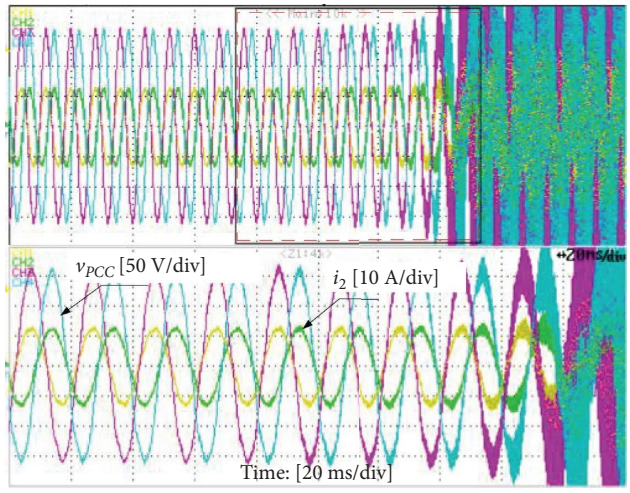

Figure 16: Measured waveforms of PCC voltages and grid currents if the HPF feedback is disabled, when $L_g = 3.6$ mH and $C_g = 2\,\mu$F.

coefficient of the proposed method is −7 and the injected damping r_1 is 6. In the steady state test, Figure 14 shows the experimental results of grid currents with the proposed controller, when $L_g = 3.6$ mH and $C_g = 2\,\mu$F. The grid currents are sinusoidal and synchronized with the PCC voltages, which gives a consistent current injection performance with analysis in the capacitive grid. It verifies the analysis that the interaction between the grid and inverter is avoided before the Nyquist frequency with the proposed control method shown in Figure 8. The dynamic responses of grid-currents are observed in Figure 15, when the reference current steps from 6.4 A to 12.8 A. The experimental results prove again that the system can achieve fast performance recovery and stable operation with proposed controller in the capacitive grid.

Figure 16 shows the measured results of PCC voltages and grid currents with the proposed control and a zoom-in view of the test results is provided when the HPF feedback loop is deactivated instantaneously. The system turns unstable because the interaction points between the grid and the inverter fall into the nonpassive region without the damping enhancement method, as shown in Figure 6. Experimental results confirm the theoretical analysis and the controller design again.

6. Conclusion

This study proposes a robust control strategy based on passivity-based control and reshaping of control output admittance within Nyquist frequency for LCL-filtered VSI. The overall conclusion can be summarized in the following points:

(1) LCL-filtered three-phase grid-tied VSI based on EL-based PBC with single inverter-side current control guarantees the robustness of the system but cannott damp the interactive resonance effectively due to the delay, especially in the capacitive grid

(2) In order to ensure the passivity of PBC-based LCL-filtered grid-tied inverter, the output admittance analysis methodology is utilized to enhance the stability and expand the passive region

(3) Even though the potential resonances can be damped effectively with capacitor current proportional feedback, there still have some nonpassive regions within Nyquist frequency. The conventional EL-based PBC method is then modified by adding a HPF feedback of the capacitor current to ensure the output control admittance which is passive within Nyquist frequency.

Finally, the simulated and experimental results are both provided from a 3 kW system to verify the effectiveness of the proposed modified controller.

Data Availability

The data used to support the findings of this study are available from the corresponding author upon request.

Conflicts of Interest

The authors declare that they have no conflicts of interest.

Acknowledgments

This study was sponsored by the Science and Technology Project of State Grid Corporation, China (No. 4000-202055048A-0-0-00).

References

[1] F. Blaabjerg, Z. Chen, and S. B. Kjaer, "Power electronics as efficient interface in dispersed power generation systems," *IEEE Transactions on Power Electronics*, vol. 19, no. 5, pp. 1184–1194, 2004.

[2] Z. Yao, Y. Zhang, and X. Hu, "Transformerless grid-connected PV inverter without common mode leakage current and shoot-through problems," *IEEE Transactions on Circuits and Systems II: Express Briefs*, vol. 67, no. 12, pp. 3257–3261, 2020.

[3] D. Pan, X. Ruan, C. Bao, W. Li, and X. Wang, "Capacitor-currentfeedback active damping with reduced computation delay for improving robustness of LCL-type grid-connected inverter," *IEEE Transactions on Power Electronics*, vol. 29, no. 7, pp. 3414–3427, 2014.

[4] R. Pēna-Alzola, M. Liserre, F. Blaabjerg, R. Sebastian, J. Dannehl, and F. W. Fuchs, "Analysis of the passive damping losses in LCL-filterbased grid converters," *IEEE Transactions on Power Electronics*, vol. 28, no. 6, pp. 2642–2646, 2013.

[5] W. Wu, Y. Sun, M. Huang et al., "A robust passive damping method for LLCL filter based grid-tied inverters to minimize the effect of grid harmonic voltages," *IEEE Transactions on Power Electronics*, vol. 29, no. 7, pp. 3279–3289, 2014.

[6] A. Kouchaki and M. Nymand, "Analytical design of passive LCL filter for three-phase two-level power factor correction rectifiers," *IEEE Transactions on Power Electronics*, vol. 33, no. 4, pp. 3012–3022, 2018.

[7] J. Dannehl, F. W. Fuchs, S. Hansen, and P. B. Thogersen, "Investigation of active damping approaches for PI-based current control of grid-connected pulse width modulation converters with LCL filters," *IEEE Transactions on Industry Applications*, vol. 46, no. 4, pp. 1509–1517, 2010.

[8] Y. He, X. Wang, X. Ruan, D. Pan, X. Xu, and F. Liu, "Capacitor-current proportional-integral positive feedback active damping for LCL-type gridconnected inverter to achieve high robustness against grid impedance variation," *IEEE Transactions on Power Electronics*, vol. 34, no. 12, Article ID 12423, 2019.

[9] M. Huang, X. Wang, P. C. Loh, and F Blaabjerg, "Active Damping of <italic>LLCL</italic>-Filter Resonance Based on <italic>LC</italic>-Trap Voltage or Current Feedback," *IEEE Transactions on Power Electronics*, vol. 31, no. 3, pp. 2337–2346, 2016.

[10] J. Xu, S. Xie, and T. Tang, "Active damping-based control for grid-connected LCL -filtered inverter with injected grid current feedback only," *IEEE Transactions on Industrial Electronics*, vol. 61, no. 9, pp. 4746–4758, 2014.

[11] Y. He, X. Wang, X. Ruan, D. Pan, and K. Qin, "Hybrid active damping combining capacitor current feedback and point of common coupling voltage feedforward for LCL-Type grid-connected inverter," *IEEE Transactions on Power Electronics*, vol. 36, no. 2, pp. 2373–2383, 2021.

[12] Y. Liu, W. Wu, Y. He, Z. Lin, F. Blaabjerg, and H. S. H Chung, "An efficient and robust hybrid damper for LCL or LLCL based grid-tied inverter with strong grid-side harmonic voltage effect rejection," *IEEE Transactions on Industrial Electronics*, vol. 63, no. 2, pp. 926–936, 2016.

[13] C. Zou, B. Liu, S. Duan, and R. Li, "Influence of delay on system stability and delay optimization of grid-connected inverters with LCL filter," *IEEE Transactions on Industrial Informatics*, vol. 10, no. 3, pp. 1775–1784, 2014.

[14] S. G. Parker, B. P. McGrath, and D. G. Holmes, "Regions of active damping control for LCL filters," *IEEE Transactions on Industry Applications*, vol. 50, no. 1, pp. 424–432, 2014.

[15] J. Wang, J. D. Yan, L. Jiang, and J. Zou, "Delay-dependent stability of single-loop controlled grid-connected inverters with *LCL* filters," *IEEE Transactions on Power Electronics*, vol. 31, no. 1, pp. 743–757, 2016.

[16] H. Komurcugil, N. Altin, S. Ozdemir, and I. Sefa, "Lyapunov-function and proportional-resonant-based control strategy for single-phase grid-connected VSI with LCL filter," *IEEE Transactions on Industrial Electronics*, vol. 63, no. 5, pp. 2838–2849, 2016.

[17] J. Wang, X. Mu, and Q. K. Li, "Study of passivity-based decoupling control of T-NPC PV grid-connected inverter," *IEEE Transactions on Industrial Electronics*, vol. 64, no. 9, pp. 7542–7551, 2017.

[18] J. Zhao, W. Wu, Z. Shuai, A. Luo, H. Sh Chung, and F. Blaabjerg, "Robust control parameters design of PBC controller for LCL-filtered grid-tied inverter," *IEEE Transactions on Power Electronics*, vol. 35, no. 8, pp. 8102–8115, 2020.

[19] Y. Chen, M. Wen, E. Lei, X. Yin, J. Lai, and Z. Wang, "Passivity-based control of cascaded multilevel converter based D-STATCOM integrated with distribution transformer," *Electric Power Systems Research*, vol. 154, pp. 1–12, 2018.

[20] J. Min, F. Ma, Q. Xu, Z. He, A. Luo, and A. Spina, "Analysis design and implementation of passivity-based control for multilevel railway power conditioner," *IEEE Transactions on Industrial Informatics*, vol. 14, no. 2, pp. 415–425, 2018.

[21] M. A. Awal, W. Yu, and I. Husain, "Passivity-based predictive-resonant current control for resonance damping in *LCL*-

e," *IEEE Transactions on Industry Applications*, vol. 56, no. 2, pp. 1702–1713, 2020.

[22] M. G. Judewicz, S. A. González, J. R. Fischer, J. F. Martinez, and D. O. Carrica, "Inverter-side current control of grid-connected voltage source inverters with LCLfilter based on generalized predictive control," *IEEE J Emerg Sel Topics Power Electron*, vol. 6, no. 4, pp. 1732–1743, 2018.

[23] X. Hao, X. Yang, T. Liu, L. Huang, and W. Chen, "A sliding-mode controller with multiresonant sliding surface for single-phase grid-connected VSI with an LCL filter," *IEEE Transactions on Power Electronics*, vol. 28, no. 5, pp. 2259–2268, 2013.

[24] M. Huang, H. Li, W. Wu, and F. Blaabjerg, "Observer-based sliding mode control to improve stability of three -phase *LCL*-filtered grid-connected VSIs," *Energies*, vol. 12, no. 8, pp. 1421–2019, 2019.

[25] R. Ortega, A. Lor, P. J. Nicklasson et al., "Passivity-based control of euler-Lagrange systems: mechanical, electrical and electromechanical applications," *Ind Robot An Internation Journal*, vol. 6, no. 3, pp. 15–28, 1998.

[26] Z. Liu, Z. Geng, and X. Hu, "An approach to suppress low frequency oscillation in the traction network of high-speed railway using passivity based control," *IEEE Transactions on Power Systems*, vol. 33, no. 4, pp. 3909–3918, 2018.

[27] X. Wang, F. Blaabjerg, and P. C. Loh, "Passivity-based stability analysis and damping injection for multiparalleled VSCs with LCL filters," *IEEE Transactions on Power Electronics*, vol. 32, no. 11, pp. 8922–8935, 2017.

[28] L. Yuxing, X. Jiazhu, S. Zhikang et al., "Passivity-based decoupling control strategy of single-phase LCL-type VSRs for harmonics suppression in railway power systems. International Journal of Electrical," *Power and Energy Systems*, vol. 117, Article ID 105698, 2020.

[29] J. Lai, X. Yin, Z. Zhang, Z. Wang, Y. Chen, and X. Yin, "System modeling and cascaded passivity based control for distribution transformer integrated with static synchronous compensator," *International Journal of Electrical Power & Energy Systems*, vol. 113, pp. 1035–1046, 2019.

[30] M. Cespedes and J. Sun, "Impedance modeling and analysis of gridconnected voltage-source converters," *IEEE Transactions on Power Electronics*, vol. 29, no. 3, pp. 1254–1261, 2014.

[31] C. Xie, K. Li, J. Zou, and J. M. Guerrero, "Passivity-based stabilization of LCL-type grid-connected inverters via a general admittance model," *IEEE Transactions on Power Electronics*, vol. 35, no. 6, pp. 6636–6648, 2020.

[32] A. Akhavan, J. C. Vasquez, and J. M. Guerrero, "A simple method for passivity enhancement of current controlled grid-connected inverters," *IEEE Transactions on Power Electronics*, vol. 35, no. 8, pp. 7735–7741, 2020.

[33] L. Harnefors, L. Zhang, and M. Bongiorno, "Frequency-domain passivity-based current controller design," *IET Power Electronics*, vol. 1, no. 4, pp. 455–465, 2008.

[34] Y. Han, M. Yang, H. Li et al., "Modeling and stability analysis of *LCL*-type grid-connected inverters: a comprehensive overview," *IEEE Access*, vol. 7, Article ID 114975, 2019.